INSTITUTE OF PHYSICS PUBLISHING SUPERCONDUCTOR SCIENCE AND TECHNOLOGY

Supercond. Sci. Technol. **18** (2005) S241–S252 doi:10.1088/0953-2048/18/12/005

# The scaling law for the strain dependence of the critical current density in $Nb_3Sn$ superconducting wires

**David M J Taylor and Damian P Hampshire**

Superconductivity Group, Physics Department, Durham University, Durham DH1 3LE, UK
and
Grenoble High Magnetic Field Laboratory, BP 166, 38042 Grenoble Cedex 9, France

E-mail: d.p.hampshire@dur.ac.uk

Received 1 September 2005, in final form 2 September 2005
Published 4 November 2005
Online at stacks.iop.org/SUST/18/S241

**Abstract**

Comprehensive measurements are reported of the critical current density ($J_C$) of internal-tin and bronze-route $Nb_3Sn$ superconducting wires as a function of magnetic field ($B \leqslant 23$ T), temperature ($4.2\ \text{K} \leqslant T \leqslant 12$ K) and axial strain ($-1.6\% \leqslant \varepsilon_I \leqslant 0.40\%$). Electric field–temperature characteristics are shown to be equivalent to the standard electric field–current density characteristics to within an experimental uncertainty of ~20 mK, implying that $J_C$ can be described using thermodynamic variables. We report a new universal relation between normalized effective upper critical field ($B^*_{C2}(0)$) and strain that is valid over a large strain range for $Nb_3Sn$ wires characterized by high upper critical fields. A power-law relation between $B^*_{C2}(0, \varepsilon_I)$ and $T^*_C(\varepsilon_I)$ (the effective critical temperature) is observed with an exponent of ~2.2 for high-upper-critical-field $Nb_3Sn$ compared to the value $\geqslant 3$ for binary $Nb_3Sn$. These data are consistent with microscopic theoretical predictions and suggest that uniaxial strain predominantly affects the phononic rather than the electronic properties of the material. The standard Summers scaling law predicts a weaker strain dependence than is observed. We propose a scaling law for $J_C(B, T, \varepsilon_I)$ based on microscopic theory and phenomenological scaling that is sufficiently general to describe materials with different impurity scattering rates and electron–phonon coupling strengths. It parametrizes complete datasets with a typical accuracy of ~4%, and provides reasonable predictions for the $J_C(B, T, \varepsilon_I)$ surface from partial datasets.

## 1. Introduction

$Nb_3Sn$ superconducting wires, which are used in almost all high-field superconducting magnets operating above 12 T [1], have a critical current density ($J_C$) that depends on the magnetic field ($B$), the temperature ($T$) and the strain-state ($\varepsilon$) of the superconductor [2–13]. Of the strain components that are generated in magnets due to thermal contraction and Lorentz forces, uniaxial strain is generally accepted to have the most significant effect on $J_C$ in $Nb_3Sn$ [14–19], and represents an area of considerable research effort. This is motivated in particular by the International Thermonuclear Experimental Reactor (ITER), which will inductively heat and confine a plasma for fusion physics applications [20–24]. There is, however, currently no consensus on the best approach to parametrizing $J_C(B, T, \varepsilon)$ data for magnet design, or on the underlying physics. Field and temperature scaling laws for $J_C$ were first observed by Fietz and Webb [25] and have underpinned a large body of experimental and theoretical work [1, 3, 26, 27]. A field and strain scaling law was developed by Ekin [6] based on $J_C$ data obtained at 4.2 K for $Nb_3Sn$ wires characterized by relatively low values of upper critical field. The first unified scaling law for $J_C(B, T, \varepsilon)$, proposed by Summers *et al* [28], combined

  

the Fietz-Webb and Ekin laws and parametrized the data available at the time quite accurately. However, following the development of apparatus capable of controlling both temperature and strain and the investigation of a number of different $Nb_3Sn$ wires, various alternative $J_C(B, T, \varepsilon)$ scaling laws have been proposed [2, 5, 17, 29–31]. One of the authors has shown that an interpolative scaling law (ISL) allows accurate parametrizations of comprehensive data for $Nb_3Al$ and $Nb_3Sn$ wires [5, 31]. However, this scaling law uses polynomial functions for the strain-dependent parameters, and therefore contains a relatively large number of empirical free parameters and cannot generally be used to extrapolate beyond the measured regions of parameter space (e.g. the measured strain range).

In this paper, a new scaling law for $J_C(B, T, \varepsilon)$ is presented that incorporates microscopic theory into the phenomenological scaling framework, thereby reducing the number of free parameters and elucidating the physical mechanisms that determine the strain effects in $Nb_3Sn$. The strain-dependent upper critical field ($B_{C2}(0, \varepsilon)$) and critical temperature ($T_C(\varepsilon)$) are accurately determined from detailed $J_C(B, T, \varepsilon)$ data for ternary $Nb_3Sn$ wires, and their relationship is analysed using microscopic theory (Eliashberg [32–38] and Ginzburg–Landau–Abrikosov–Gor'kov theory [39–41], adopting a similar approach to Welch [14]). Hence an empirically and theoretically justified scaling law is obtained with a number of important differences to previous scaling laws [2, 28] that can be understood in terms of the different impurity scattering rates in binary and ternary $Nb_3Sn$. Furthermore, a comparison between the theory and the experimental results allows us to address the question that has been investigated by a number of authors concerning whether the uniaxial strain effects in $Nb_3Sn$ are predominantly due to changes in the electronic or the phononic properties of the material [14, 35, 42–45].

The paper is structured as follows: in section 2, the experimental techniques are summarized. Section 3 contains the main experimental results, presenting detailed $J_C(B, T, \varepsilon)$ data for the internal-tin and bronze-route wires used in the ITER model coils. These data are subject to various consistency tests, and then parametrized using the interpolative scaling law and the strain dependence of the superconducting parameters described. In section 4, the observed relationships between $B_{C2}(0)$ and $T_C$ are examined using microscopic theory. Finally, in section 5, the new scaling law is presented and its accuracy in parametrizing complete and partial $J_C(B, T, \varepsilon)$ datasets is considered.

## 2. Experimental techniques

Detailed measurements were made on two types of 0.81 mm diameter multifilamentary $Nb_3Sn$ wire: an internal-tin wire made by Europa Metalli-LMI and a bronze-route wire made by Vacuumschmelze. The wires were subject to standard heat-treatments (terminating at 650 °C for 175–200 h) [46], and then etched in hydrochloric acid to remove the chromium plating and transferred to copper–beryllium 'helical-spring' sample holders [47, 48], to which they were attached by copper-plating and soldering. The experiments were carried out using our strain probe [31, 49], which can twist one end of the spring with respect to the other and hence apply an axial strain to the wire. The strain values quoted characterize the average strain in the wire. They are calculated using data from strain-gauge calibrations, with correction factors of ∼2% (tee-shaped springs) and ∼9% (rectangular springs) obtained from finite element analysis to account primarily for the strain gradient across the wire [48]. Measurements at 4.2 K were made with the sample directly immersed in a liquid-helium bath. At temperatures above 4.2 K, the sample was located in a variable-temperature enclosure with three independently controlled Cernox thermometers and constantan wire heaters [50]. The voltage ($V$) across a section of the wire (typical length ∼ 20 mm) was measured using a nanovolt amplifier and a digital voltmeter, with most of the measurements being made at constant temperature ($T$) with a slowly increasing current ($I$), although some additional measurements on the first internal-tin sample were made at constant current with a slowly increasing temperature.

For the first internal-tin sample, $V$–$I$ measurements were made at 4.2 K at applied strains from 0.49% tension to −0.48% compression and magnetic field up to 15 T. The applied strain was then set to zero and the probe was warmed to room temperature so that the variable-temperature enclosure could be fitted. The probe was then cooled back to 4.2 K and the applied strain was changed to −0.48% (−0.76% intrinsic strain) where $V$–$I$ and $V$–$T$ measurements were carried out. $V$–$I$ measurements were then made at different applied strains from −0.48% to 0.61% and then to −0.81%. The second internal-tin sample was measured in magnetic fields up to 23 T in a resistive magnet at the European high-field laboratory in Grenoble, where $V$–$I$ data were obtained at a temperature of 4.2 K at applied strains between +0.49% and −0.48%. For the bronze-route wire, $V$–$I$ measurements were carried out at 4.2 K in fields up to 15 T (sample 1), at 8 and 12 K in fields up to 15 T (sample 2) and at 4.2 K in fields up to 23 T in Grenoble (sample 3). In agreement with previous results [30, 46, 48], the data were generally found to be reversible to within ∼4% after the applied strain cycles. There were no significant differences between the results for different samples of the same wire: for example, equivalent $J_C$ data at fields ⩽ 15 T obtained in Durham and Grenoble agree to within ∼2%.

The paper provides engineering critical current density ($J_C$) data calculated by dividing the critical current ($I_C$) by the total cross-sectional area of the wire ($5.153 \times 10^{-7}$ m$^2$) and defined at an electric-field criterion of 10 $\mu$V m$^{-1}$. $J_C$ was calculated using the value of current in the wire alone, obtained by subtracting the current in the normal shunt (typically 50 mA) from the total current [51].

## 3. Experimental results and preliminary analysis

### 3.1. Interlaboratory comparisons

Interlaboratory comparisons of variable-strain $J_C$ data for the internal-tin and bronze-route wires and cables are shown in figure 1, where the normalized critical current at 4.2 K and 13 T is plotted as a function of intrinsic strain. Intrinsic strain (generally assumed to be the total axial strain on the superconducting filaments) is defined as [11, 35, 48, 52]

$$\varepsilon_I = \varepsilon_A - \varepsilon_M, \tag{1}$$

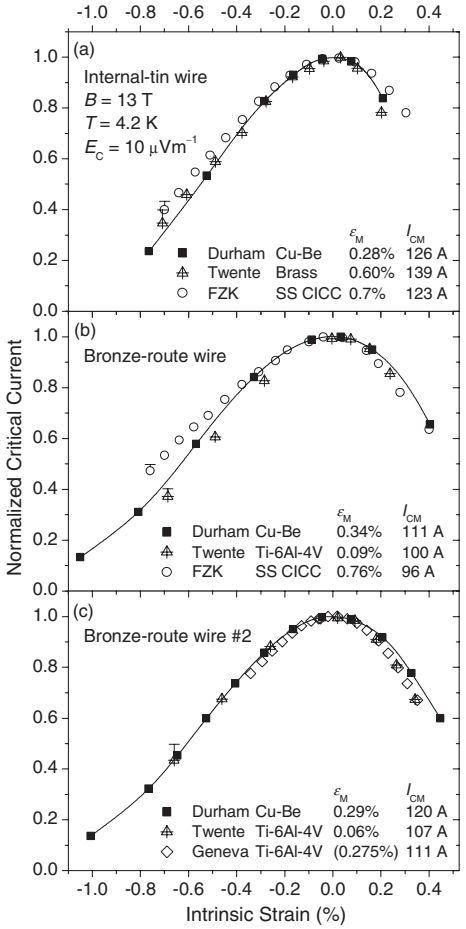


**Figure 1.** Interlaboratory comparisons of the normalized critical current as a function of intrinsic strain at 4.2 K and 13 T for (a) internal-tin (EM-LMI), (b) bronze-route (Vac) and (c) second bronze-route (Furukawa) ITER $Nb_3Sn$ wires. Critical currents were measured at 10 $\mu$V m$^{-1}$ or calculated at 10 $\mu$V m$^{-1}$ from measurements performed at higher electric-field criteria using $n$-values measured in Durham (the error bars show the effect of these calculations on the normalized values). The legends show the spring material (or the CICC jacket material), the value of applied strain where the critical current is a maximum ($\varepsilon_M$) and the value of the critical current at this maximum ($I_{CM}$) [29, 53–55, 92].

where $\varepsilon_A$ is the applied strain and $\varepsilon_M$ is the value of applied strain at the peak in $J_C$. Figure 1 also shows data for a second bronze-route wire manufactured by Furukawa [53]. The measurements in other laboratories were performed on individual wires at the University of Twente using a different type of 'bending spring' [29], at the University of Geneva using a helical spring [54] and on cable-in-conduit conductors (CICCs) at Forschungszentrum Karlsruhe using an 'axial pull' system [55]. It can be seen that the agreement between the normalized critical current data from different laboratories is generally good: for measurements on single wires, typical variations are ±5%, although the CICC data are less strain-sensitive in compression. We have particular confidence in our internal-tin wire data because six different samples on springs of various materials and geometries all show a similar intrinsic strain dependence for $J_C$ to within ±5% [46, 48]. These results demonstrate the reliability and generality of the data prior to comparisons with theory.

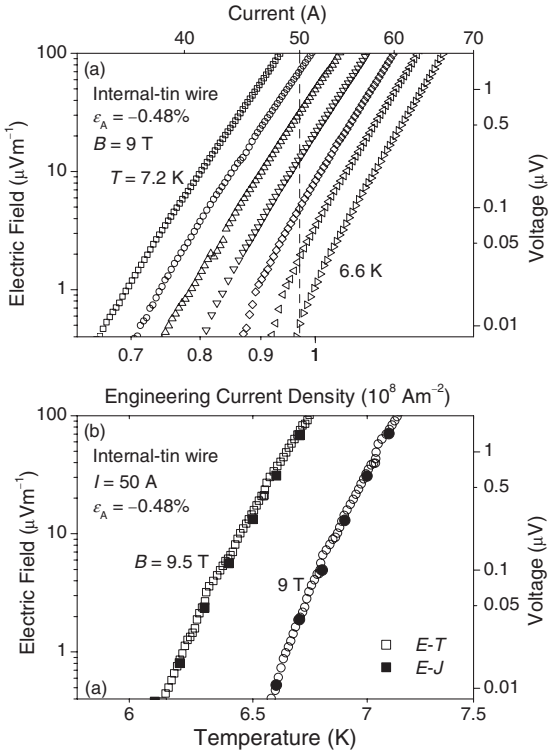


**Figure 2.** Log–log plots for the internal-tin (EM-LMI) wire at −0.48% applied strain of (a) electric field versus engineering current density at 9 T and at 0.1 K increments between 6.6 and 7.2 K, and (b) electric field versus temperature at a constant total current of 50 A and at 9 and 9.5 T. In (b), the open symbols show the $E$–$T$ characteristics, while the closed symbols show points extracted from the $E$–$J$ characteristics (e.g. on the dashed line in (a)).

### 3.2. *E–J and E–T characteristics*

Figure 2(a) shows the electric field–engineering current density ($E$–$J$) characteristics for the internal-tin wire at −0.48% applied strain, at a magnetic field of 9 T and at 0.1 K temperature increments. Figure 2(b) shows the electric field–temperature ($E$–$T$) characteristics for a total current of 50 A and magnetic fields of 9 and 9.5 T, together with equivalent $E(J, B, T, \varepsilon)$ data points taken from $E$–$J$ characteristics. Figure 3(a) compares $J_C$ and $T_{CS}$ (current-sharing temperature [22, 56]) data obtained from $E$–$J$ and $E$–$T$ characteristics at an electric-field criterion of 10 $\mu$V m$^{-1}$ throughout the superconducting phase. It can be seen that the data superimpose, with a typical uncertainty of ∼20 mK.

The $E$–$J$ data can be parametrized by the standard power-law expression [57]:

$$E(J, B, T, \varepsilon) = E_C[J/J_C(B, T, \varepsilon)]^n, \qquad (2)$$

where the $n$-value for the internal-tin wire is approximately constant over one order of magnitude of electric field (at constant $B$, $T$ and $\varepsilon$), but decreases slowly with increasing electric field. The $E$–$T$ characteristics can also be described by a power law, where the exponent is again approximately constant over one order of magnitude of electric field (we note, however, that an exponential dependence gives a similarly accurate parametrization [58]). Figure 3(b) shows a

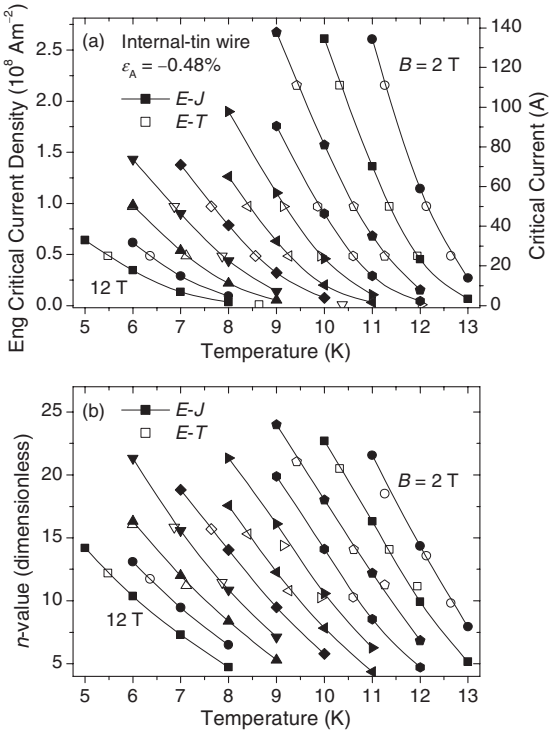


**Figure 3.** (a) Engineering critical current density (and critical current) and (b) $n$-value as a function of temperature at integer magnetic fields between 2 and 12 T. The closed symbols show the results obtained from the $E$–$J$ characteristics, while the open symbols show the results calculated from the $E$–$T$ characteristics. $J_C$ values were determined at 10 $\mu$V m$^{-1}$ and $n$-values in the range 10–100 $\mu$V m$^{-1}$. The values were calculated using the total current (including the shunt current); hence, the $n$-values are typically ∼0.75 lower than the shunt-subtracted values.

comparison of $n$-values obtained from the $E$–$J$ characteristics (for electric fields between 10 and 100 $\mu$V m$^{-1}$) and calculated from the exponent of the $E$–$T$ characteristics ($\partial \log E / \partial \log T$) via the following expression:

$$\left.\frac{\partial \log E}{\partial \log T}\right|_{T=T_{CS}} = \left.\left(\frac{\partial \log E}{\partial \log J_C}\frac{\partial \log J_C}{\partial \log T}\right)\right|_{T=T_{CS}} = -n\frac{T_{CS}}{J_C}\left.\frac{\partial J_C}{\partial T}\right|_{T=T_{CS}}. \quad (3)$$

The data lie on a single curve to within ∼100 mK, which corresponds to systematic changes in temperature during the transition (10–100 $\mu$V m$^{-1}$) of ∼10 mK. Unpublished data for a number of ITER-candidate wires show that, in high magnetic fields, $J_C$ is also a non-hysteretic function of applied magnetic field and temperature, consistent with other data in the literature on similar wires [59] and unlike some high-temperature superconductors or granular materials [60–62]. Figures 3(a) and (b) together demonstrate that $E(J, B, T, \varepsilon)$ (i.e. $J_C(B, T, \varepsilon)$ at arbitrary electric-field criteria) is a path-independent, single-valued function. This implies that $E$–$T$ measurements of $J_C(B, T, \varepsilon)$ made in large model coils should be consistent with $E$–$J$ measurements on the component wires [22, 56], and that $J_C$ can in principle be described using thermodynamic variables.

### *3.3. $J_C(B, T, \varepsilon)$ data parametrized using the interpolative scaling law*

The $J_C(B, T, \varepsilon)$ data can be parametrized using the interpolative scaling law (ISL) [5] in which the volume pinning force ($F_P = J_C B$) is given by [26]

$$F_P = \frac{A'(\varepsilon)[B^*_{C2}(T, \varepsilon)]^n}{[\kappa^*_1(T, \varepsilon)]^m} b^p (1 - b)^q, \quad (4)$$

where $b = B/B^*_{C2}(T, \varepsilon)$ and $B^*_{C2}(T, \varepsilon)$ is the effective upper critical field, which is parametrized by

$$B^*_{C2}(T, \varepsilon) = B^*_{C2}(0, \varepsilon)(1 - t^\nu). \quad (5)$$

Here, $t = T/T^*_C(\varepsilon)$ and $T^*_C(\varepsilon)$ is the effective critical temperature. $\kappa^*_1(T, \varepsilon)$ is the Ginzburg–Landau parameter given by [5]

$$\kappa^*_1(T, \varepsilon) = \frac{1.03[\eta(\varepsilon)]^{1/2} B^*_{C2}(T, \varepsilon)}{\mu_0^{1/2}[\gamma(\varepsilon)]^{1/2} T^*_C(\varepsilon)(1 - t^2)}, \quad (6)$$

where $\eta(\varepsilon) = 1 - 12.2(k_B T_C/\hbar\omega_{ln})^2 \ln(\hbar\omega_{ln}/3k_B T_C)$ is a strong-coupling correction to the BCS value of the ratio $\mu_0\gamma T_C^2/[B_C(0)]^2$ ($\omega_{ln}$ is an average phonon frequency) and $\gamma(\varepsilon)$ is the electronic specific heat coefficient [5, 33, 40]. Combining equations (4) and (6), incorporating $A'(\varepsilon)$, $\eta(\varepsilon)$ and $\gamma(\varepsilon)$ into a single strain-dependent parameter $A(\varepsilon)$ and setting $m = 2$ (similarly to previous work [3, 5, 31]) results in the following expression for $J_C(B, T, \varepsilon)$:

$$J_C(B, T, \varepsilon) = A(\varepsilon)[T^*_C(\varepsilon)(1 - t^2)]^2 \times [B^*_{C2}(T, \varepsilon)]^{n-3} b^{p-1}(1 - b)^q. \quad (7)$$

The scaling law therefore involves the exponents $n$, $p$, $q$ and $\nu$, and the parameters $A(\varepsilon)$, $T^*_C(\varepsilon)$ and $B^*_{C2}(0, \varepsilon)$. These strain-dependent parameters are constrained to be fourth-order polynomial functions of applied strain with a stationary point (e.g. maximum) at a common value, $\varepsilon_M$.

The interpolative scaling law is found to enable extremely accurate parametrizations of the $J_C$ data over the large ranges of magnetic field, temperature and strain that were investigated. The RMS differences between the measured and calculated values are 1.40 A for the internal-tin wire and 2.05 A for the bronze-route wire. The parametrizations are compared graphically with the measured $J_C(B, T, \varepsilon)$ data in figures 4 and 5. Figure 4 also shows a comparison between the measured data for the internal-tin wire and the values for $J_C(12\text{ T}, 4.2\text{ K}, \varepsilon_I)$ calculated using the standard Summers scaling law [28, 63], with the free parameters obtained by fitting the data for $|\varepsilon_I| < 0.22\%$. Summers predicts a weaker strain dependence for $J_C$ than is observed experimentally for both the internal-tin wire and the bronze-route wire (comparison not shown)—typical RMS differences are ∼10 A [23, 24]. It will be shown in sections 3.4 and 4.1 that the expressions used in the standard Summers scaling law [28, 63] for the strain dependence of the superconducting parameters and their interrelationship are not valid for ternary, high-upper-critical-field $Nb_3Sn$.

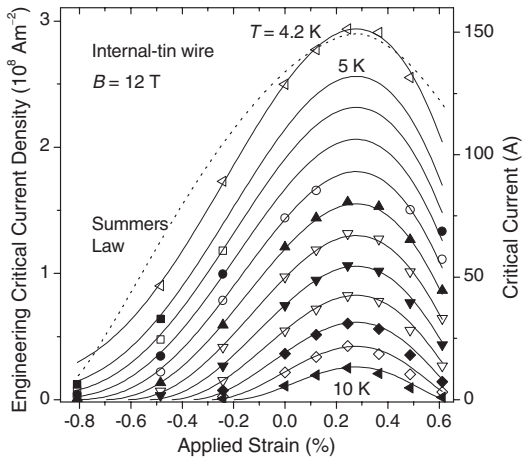


**Figure 4.** Engineering critical current density (and critical current) of the internal-tin (EM-LMI) wire as a function of applied strain at 12 T and at 4.2 K and 0.5 K increments between 5 and 10 K. The symbols show the measured data, the solid lines the interpolative scaling law and the dotted line the Summers scaling law (obtained by fitting the $J_C(B, T, \varepsilon)$ data for $|\varepsilon_1| < 0.22\%$).

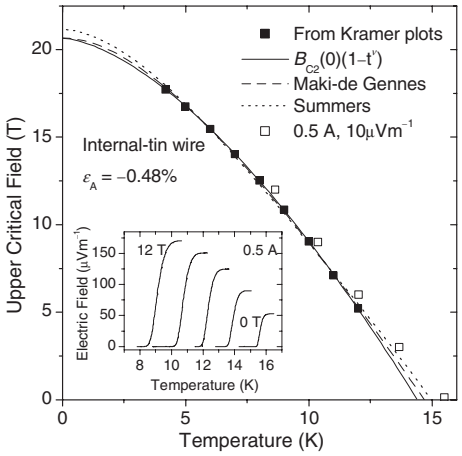


**Figure 6.** Upper critical field as a function of temperature for the internal-tin (EM-LMI) wire at −0.48% applied strain (i.e. close to the operating strain of the TFMC [23]). The closed symbols show $B^*_{C2}$ obtained from Kramer plots (see figure 7) and the lines show various fits to these data. Also shown are the values of $B^{\rho}_{C2}$ (open symbols) determined at 0.5 A and 10 $\mu$V m$^{-1}$ from the $E$–$T$ data shown in the inset.

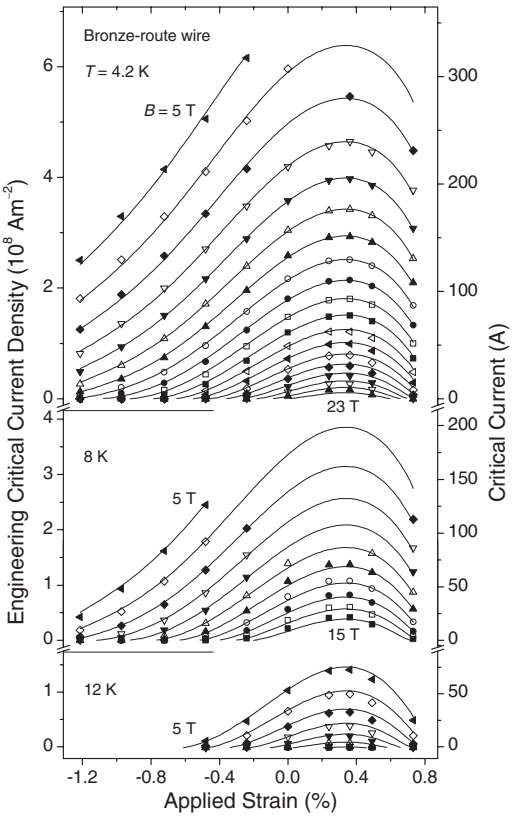


**Figure 5.** Engineering critical current density (and critical current) of the bronze-route (Vac) wire as a function of applied strain at integer magnetic fields between 5 and 23 T and at 4.2, 8 and 12 K. The symbols show the measured data and the solid lines the interpolative scaling law.

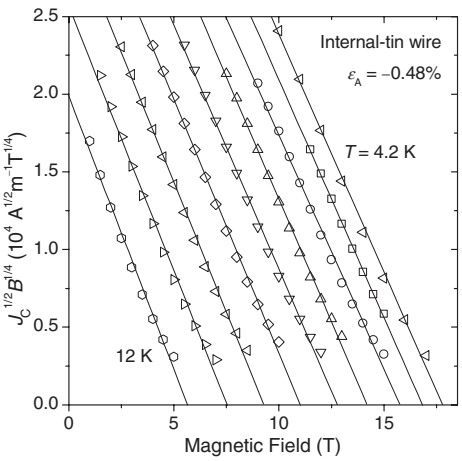


**Figure 7.** Kramer plots for the internal-tin (EM-LMI) wire at −0.48% applied strain and at 4.2 K and 1 K increments between 5 and 10 K. The symbols show the measured data, and the lines the best straight-line fits.

### *3.4. The strain dependence of $B_{C2}$ and $T_C$*

Figure 6 shows the upper critical field as a function of temperature for the internal-tin wire at −0.48% applied strain (close to the estimated strain in the ITER toroidal field model coil [22, 23]). The $B^*_{C2}(T, \varepsilon)$ data were obtained from the Kramer plots in figure 7, where the good straight-line fits demonstrate that in this case the magnetic field dependence of $J_C$ can be parametrized with $p = 1/2$ and $q = 2$ (at least for $I_C > 1$ A) [27]. It can be seen that equation (5) with $\nu \approx 1.5$ provides a good fit to the $B^*_{C2}(T, \varepsilon)$ data. Two other fits to these data are also shown: the Maki–de Gennes relation for a dirty superconductor with no Pauli paramagnetic limiting [39, 64, 65], and the Summers scaling law relation [28]. Also shown in figure 6 are the values of upper critical field ($B^{\rho}_{C2}(T, \varepsilon)$) determined at a current of 0.5 A and an electric-field criterion of 10 $\mu$V m$^{-1}$ (5–20% of the transition height). These low-current-density values of $B_{C2}$ and $T_C$ are ∼0.75 T and ∼0.8 K higher than the values obtained from the Kramer plots (and equation (5)). At this value of strain, the

measured $J_C$ goes to zero less rapidly than the Kramer lines, with a 'tail' that is usually associated with the distribution of $T_C$ and $B_{C2}$ in technological wires [5, 66]. A reasonable interpretation of the difference is that the scaling law values of $B^*_{C2}$ and $T^*_C$ are characteristic values for the bulk of the material (they are relatively insensitive to the low-$J_C$ values in the tail), while the resistivity values give the maxima (or 'best parts') of the distributions in $B_{C2}$ and $T_C$ [5, 6, 67, 68]. The distributions can be attributed to composition gradients across the filaments [66, 68].

Figure 8(a) shows normalized values of $B^*_{C2}(0, \varepsilon_I)$ for the internal-tin and bronze-route wires, as well as additional data for the second bronze-route wire (Furukawa) [53] and a modified jelly roll (MJR) wire [5]. $B^*_{C2}(0, \varepsilon_I)$ follows an approximately universal relation, which is largely independent of the choice of $p$ and $q$ [6]. Figure 8(a) also includes two different datasets obtained from the literature, represented by best-fit lines [6, 42]. These values were calculated from the $B^*_{C2}(4.2\ \mathrm{K}, \varepsilon_I)$ data using equations (5) and (8), although the differences between the normalized values of $B^*_{C2}$ at $T = 0$ and 4.2 K are not large (the values for the second bronze-route wire were also calculated in this way) [28]. The less strain-sensitive line taken from Ekin's well known work represents relatively clean $Nb_3Sn$ with low values of $B^*_{C2}(0, \varepsilon_I = 0)$ of ∼24 T [6], while the more strain-sensitive line is for $Nb_3Sn$ wires with Ta additions and higher values of $B^*_{C2}(0, \varepsilon_I = 0)$ [42]. The differences between binary and ternary $Nb_3Sn$ are predicted by microscopic theory (see section 4.2) and have been noted previously [1, 42, 69, 70]. The ITER-candidate and other recently developed $Nb_3Sn$ wires have ternary additions of Ti (the internal-tin wire) or Ta (the bronze-route wire) and relatively high values of $B^*_{C2}(0, \varepsilon_I = 0)$: typically 28–30 T. Hence the better agreement with the previous ternary data rather than the binary data correlates with the higher values of $B^*_{C2}(0, \varepsilon_I = 0)$. The higher strain-sensitivity of $J_C$ for the internal-tin wire in relation to the other wires (see figure 1) is due to lower absolute values of $B^*_{C2}(0)$ and $T^*_C$ at zero intrinsic strain (see section 5).

Figure 8(b) shows normalized values of $T^*_C(\varepsilon_I)$ for the internal-tin, bronze-route and MJR wires and $T^\rho_C(\varepsilon_I)$ data obtained from resistivity measurements for the MJR wire. The $T^\rho_C(\varepsilon_I)$ data and $B^\rho_{C2}(T, \varepsilon)$ data (not shown) are less strain-sensitive than the scaling-law values—behaviour that is observed in all of the wires we have investigated and can be related to strain (and temperature) variations in the low-current-density tails discussed above.

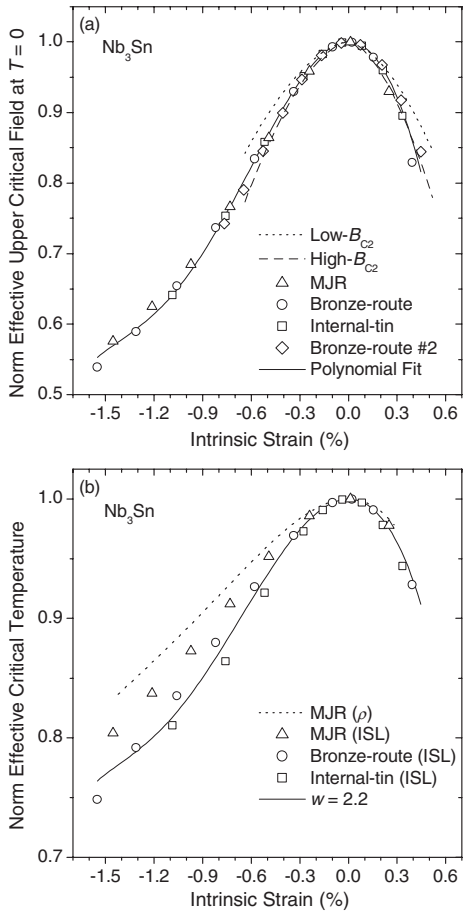


**Figure 8.** (a) The normalized effective upper critical field at $T = 0$ and (b) normalized effective critical temperature as a function of intrinsic strain for different $Nb_3Sn$ wires. In (a), the symbols show data for wires measured in Durham and the solid line shows a universal fit to these data, while the dotted line is for previous measurements on low-$B^*_{C2}(0)$ wires [6] and the dashed line for high-$B^*_{C2}(0)$ wires [42]. For the second bronze-route (Furukawa) data and the dashed and dotted lines, $B^*_{C2}(0)$ was calculated from the $B^*_{C2}(4.2\ \mathrm{K})$ data using equations (5) and (8). In (b), the solid line is calculated using the universal fit to the normalized $B^*_{C2}(0)$ data and the power-law relation with $w = 2.2$, while the dotted line shows $T^\rho_C(\varepsilon_I)$ data obtained from resistivity measurements for the MJR wire.

## 4. Relationship between strain-dependent superconducting parameters

### *4.1. Power-law relationship and experimental data*

An empirical power-law relationship between $B_{C2}(0, \varepsilon_I)$ and $T_C(\varepsilon_I)$ was first proposed by Ekin (although originally in terms of the upper critical field at 4.2 K) [6]:

$$\frac{B_{C2}(0, \varepsilon_I)}{B_{C2}(0, \varepsilon_I = 0)} = \left(\frac{T_C(\varepsilon_I)}{T_C(\varepsilon_I = 0)}\right)^w. \qquad (8)$$

The exponent $w \approx 3$ was estimated by combining $B^*_{C2}(4.2\ \mathrm{K}, \varepsilon_I)$ data obtained from $J_C$ measurements on binary $Nb_3Sn$ wires [6] with $T^\chi_C(\varepsilon_I)$ data (available in the literature at the time) from susceptibility measurements on a different set of binary $Nb_3Sn$ wires [11]. The power law with $w = 3$ is currently used in a number of scaling laws for $J_C(B, T, \varepsilon)$, including the Summers law [2, 28, 63]. The original (low-$B^*_{C2}$) data give a value of $w = 3.8$ if the upper-critical-field data at 4.2 K are used directly. In figure 9(a), we plot $B^*_{C2}(0, \varepsilon_I)$ values calculated from the $B^*_{C2}(4.2\ \mathrm{K}, \varepsilon_I)$ and $T^\chi_C(\varepsilon_I)$ data using the Maki–de Gennes relation: in this case, the best fit gives $w = 3.6$. Assuming that $T^\chi_C(\varepsilon_I)$ and $T^\rho_C(\varepsilon_I)$ behave similarly, the different strain dependences presented in this work for scaling-law and resistivity data imply that high values of $w$ are partly a result of combining $B^*_{C2}$ and $T^\chi_C$ data. Also shown in figure 9(a) are values obtained from low-current-density measurements of $B^\rho_{C2}(T, \varepsilon_I)$ for the bronze-route $Nb_3Sn$ wire ($I = 0.5$ A), the MJR $Nb_3Sn$ wire (30 mA) [5] and a jelly-roll $Nb_3Al$ wire

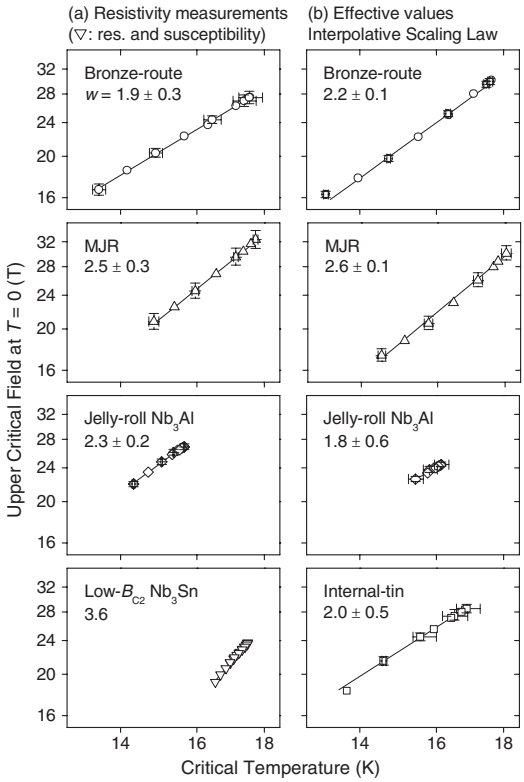


**Figure 9.** Log–log plots of upper critical field at $T = 0$ versus critical temperature for different $A15$ wires: (a) data from resistivity and other measurements; (b) effective values obtained by fitting the $J_C$ data using the interpolative scaling law [5]. The solid lines show the best power-law fits and the legend shows the values of the exponent $w$. (All panels have the same scale.)

(30 mA) [31], where equation (5) was used to extrapolate to $T = 0$ and $B = 0$. It can be seen that for these $A15$ wires, the values of $w$ are all between ∼1.9 and ∼2.5. In addition, figure 9(b) shows the values of $B^*_{C2}(0, \varepsilon_I)$ and $T^*_C(\varepsilon_I)$ obtained using the interpolative scaling law from the comprehensive $J_C(B, T, \varepsilon)$ datasets available for four different $A15$ wires. These are also consistent with the power law and give similar values of $w$, despite the different strain dependences observed (see section 3.4). This implies that distributions in $B_{C2}$ and $T_C$ due to composition gradients, for example, do not have a significant effect on the exponent $w$. For $Nb_3Sn$ wires characterized by high values of $B^*_{C2}(0, \varepsilon_I = 0)$ (approximately 28–30 T), the values of $w \leqslant 2.5$ are significantly lower than the values ($w \geqslant 3$) obtained for binary, low-$B^*_{C2}$ (∼24 T) $Nb_3Sn$ wires.

### *4.2. Analysis using microscopic theory*

The Allen and Dynes equation gives the critical temperature of strongly coupled superconductors in terms of various microscopic parameters [32, 34]:

$$k_B T_C = \frac{f_1 f_2 \hbar \omega_{ln}}{1.20} \exp\left(-\frac{1.04(1+\lambda)}{\lambda - \mu^* - 0.62\lambda\mu^*}\right), \qquad (9)$$

where $\omega_{ln}$ is a weighted logarithmically averaged phonon frequency, $\lambda$ is the electron–phonon coupling parameter, $\mu^*$ is the effective Coulomb-repulsion parameter, and $f_1$ and $f_2$ are correction factors of order unity [32]. Alternative $T_C$ equations have been proposed, including one by Kresin [36–38] which is also considered below. The electron–phonon coupling parameter is related to the bare electronic density of states at the Fermi energy $N(0)$ and a weighted RMS phonon frequency $\omega_2$ by [34]:

$$\lambda = \frac{N(0)\langle I^2\rangle}{M\omega_2^2}, \qquad (10)$$

where $\langle I^2\rangle$ is the average over the Fermi surface of the electron–phonon matrix element squared and $M$ is the average ionic mass. The electronic specific heat coefficient $\gamma$ is related to $N(0)$ and $\lambda$ by [34]

$$\gamma = \tfrac{2}{3}\pi^2 k_B^2 N(0)(1+\lambda). \qquad (11)$$

**Table 1.** Microscopic parameters determined from tunnelling measurements on $Nb_3Sn$ [71] and $Nb_3Al$ (23 at.% Al) [72]. Also shown are the values of $T_C$ calculated using equation (9) with the measured values of $\omega_{ln}$, $\lambda$ and $\mu^*$, and the values of $\mu^*$ calculated using the measured values of $\omega_{ln}$, $\lambda$ and $T_C$.

| | $Nb_3Sn$ | $Nb_3Al$ |
|---|---|---|
| $\omega_{ln}$ (meV) | 10.8 | 9.5 |
| $\omega_2$ (meV) | 15.0 | 13.5 |
| $\lambda$ | $1.8 \pm 0.15$ | $1.7 \pm 0.05$ |
| $\mu^*$ meas. (calc.) | $0.16 \pm 0.03$ (0.14) | $0.15 \pm 0.02$ (0.10) |
| $T_C$ (K) calc. (meas.) | 16.2 (17.5) | 13.9 (16.4) |

The parameters $\omega_{ln}$, $\omega_2$, $\lambda$ and $\mu^*$ determined from tunnelling measurements on $Nb_3Sn$ [71] and off-stoichiometric $Nb_3Al$ [72] are shown in table 1. In the analysis described below, we will use $\mu^*$ as a free parameter to fit the measured zero-intrinsic-strain values of $T_C$, which can generally be achieved with relatively small changes in $\mu^*$ (see table 1) [40]. We will make the assumption that the variations of $\mu^*$ or $\langle I^2\rangle$ with strain are considerably less important than the other parameters, and hence they can be considered as constants. We will also assume that the strain dependence of the normalized average phonon frequencies ($\omega_{ln}$ and $\omega_2$) is the same [19]. These assumptions are discussed in more detail in section 4.3.

The variation of $T_C$ with uniaxial strain can be related to variations in the average phonon frequencies and/or variations in the bare electronic density of states at the Fermi energy. Due to a lack of detailed information in the literature about the uniaxial strain dependence of these parameters, we will begin by considering the two extreme cases: firstly that the strain dependence of $T_C$ is entirely due to the strain dependence of the average phonon frequencies, and secondly that strain only affects electronic properties (i.e. $N(0)$). For $Nb_3Sn$, figure 10 shows how $T_C$ varies in these two cases: $T_C$ decreases approximately linearly as either $\omega_{ln}$ increases or $N(0)$ decreases. In both cases, a decrease in $T_C$ of 23% (corresponding to $\varepsilon_I = -1.55\%$ for the bronze-route wire) is caused by a change of ∼20% in $\omega_{ln}$ or $N(0)$. Figure 10 also shows the results obtained using the Kresin $T_C$ equation (together with equation (10)) [36–38] for the case where only phononic changes occur. These results agree to within ∼3% with those obtained using the Allen and Dynes equation (a similar agreement is also observed for changes only in $N(0)$—not shown), which, given our assumption of identical strain dependences for $\omega_{ln}$ and $\omega_2$, is to be expected as both equations

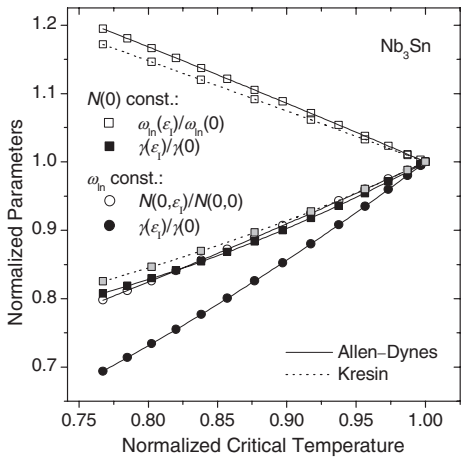


**Figure 10.** Calculated microscopic parameters for $Nb_3Sn$ as a function of critical temperature, with all quantities normalized to their values at zero intrinsic strain. Square symbols, $\omega_{ln}$ and $\gamma$ calculated assuming constant $N(0)$; round symbols, $N(0)$ and $\gamma$ calculated assuming constant $\omega_{ln}$. The calculation assumes that $\mu^*$ and $\langle I^2 \rangle$ are constant and that the strain dependence of the normalized values of $\omega_{ln}$ and $\omega_2$ is the same [19]. The data connected by solid curves are calculated using the Allen and Dynes equation (equation (9)); the data connected by dotted curves are calculated using the Kresin $T_C$ equation [36–38]. The maximum reduction in critical temperature (23%) corresponds to the measured reduction for the bronze-route (Vac) wire at −1.55% intrinsic strain.

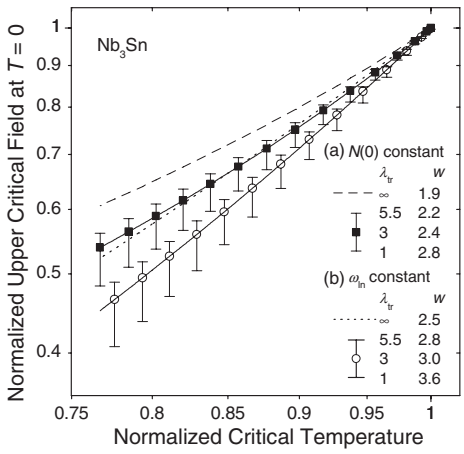


**Figure 11.** Log–log plot of the calculated upper critical field at $T = 0$ versus critical temperature for $Nb_3Sn$, with both quantities normalized to their values at zero intrinsic strain. Two cases are considered: (a) $N(0)$ is constant and $\omega_{ln}$ and $\omega_2$ vary with uniaxial strain, and (b) $\omega_{ln}$ and $\omega_2$ are constant and $N(0)$ varies with strain. The symbols are for $\lambda_{tr}(\varepsilon_I = 0) = 3$, the error bars for $\lambda_{tr}(\varepsilon_I = 0) = 5.5$ and 1 at their extrema and the dotted and dashed lines for $\lambda_{tr}(\varepsilon_I = 0) = \infty$ (extreme dirty limit). All data are calculated using the Allen and Dynes equation; the Kresin $T_C$ equation gives values of $w$ that are lower by ∼0.1. The maximum reduction in critical temperature (23%) corresponds to the measured reduction for the bronze-route (Vac) wire at −1.55% intrinsic strain.

are valid for $Nb_3Sn$ with $\lambda \approx 1.8$ [19, 73, 74]. The data shown in figure 10 are calculated for $Nb_3Sn$ with $T_C(\varepsilon_I = 0) = 17.5$ K (bronze-route wire), but the relationships between the reduced parameters and the reduced critical temperature are insensitive (to within ∼1%) to quite large variations in $T_C(\varepsilon_I = 0)$ (∼1 K). These relationships are also similar (to within ∼1%) for $Nb_3Al$, although the critical temperature of $Nb_3Al$ is a factor of ∼3 less sensitive to uniaxial strain [31].

The upper critical field at $T = 0$ can be calculated using the following expression [39–41]:

$$B_{C2}(0) = 0.973\mu_0^{1/2}\eta_{B_{C2}(0)}\kappa^*(0,\lambda_{tr})[R(\lambda_{tr})]^{-1} \times [7.30 \times 10^{37}(\gamma T_C/S)^2 + 2.78 \times 10^6 \gamma T_C \rho_n], \quad (12)$$

where $\eta_{B_{C2}(0)}$ is a strong-coupling correction of order unity [40], $\kappa^*$ is the reduced temperature-dependent Ginzburg–Landau parameter ($\kappa^*(0,0) = 1.26$ and $\kappa^*(0,\infty) = 1.20$), $R(\lambda_{tr})(1+\lambda_{tr})^{-1}$ is the Gor'kov function ($R(0) = 1$ and $R(\infty) = 1.17$), $\lambda_{tr}$ is the reduced mean collision frequency given by [41]:

$$\lambda_{tr} = 0.882\xi_0^*/l_{tr} = 3.81 \times 10^{-32} S^2 \rho_n/(\gamma T_C). \quad (13)$$

$\xi_0^*$ is the renormalized BCS coherence length, $l_{tr}$ is the electron mean free path, $S$ is the Fermi surface area, and $\rho_n$ is the low-temperature normal-state resistivity. We note that although equation (12) neglects Pauli limiting and spin–orbit scattering [75, 76], this is justified both experimentally [41, 77] and theoretically [40] for some strongly coupled superconductors including $Nb_3Sn$, as discussed in the excellent review by Carbotte [40].

Both $S$ and $\rho_n$ are expected to be largely independent of uniaxial strain, and are considered as constants with $S = (1.7 \pm 0.7) \times 10^{21}$ m$^2$ for $Nb_3Sn$ [41] and $(1.8 \pm 0.7) \times 10^{21}$ m$^2$ for $Nb_3Al$ [78]. Analysis of data for monofilamentary bronze-route $Nb_3Sn$ wires [79] shows that $\lambda_{tr}(\varepsilon_I \approx 0) = 3 \pm 2.5$ for materials with tertiary additions (Ti, Ta) and optimal upper critical fields, which are similar to the technological wires that we have measured (the uncertainty in $\lambda_{tr}$ given here is calculated from the uncertainty in $S$). By setting $\lambda_{tr}(\varepsilon_I = 0) = 3$, the variation of $B_{C2}(0)$ can be calculated using equations (12) and (13), with $\gamma(\varepsilon_I = 0)$ and $\rho_n$ calculated from the measured value of $B_{C2}(0)$ at zero intrinsic strain (for the bronze-route wire with $B_{C2}(0, \varepsilon_I = 0) = 27.6$ T, we get values consistent with the literature [41], $\rho_n = 41\ \mu\Omega$ cm and $\gamma(\varepsilon_I = 0) = 860$ J m$^{-3}$ K$^{-2}$, although the conclusions given below are independent of the precise values of $B_{C2}(0,0)$).

For $\lambda_{tr} \leqslant 1$ (the 'clean limit') the first term in the square brackets in equation (12) dominates and $B_{C2}(0) \propto (\gamma T_C)^2$, whereas for $\lambda_{tr} \geqslant 1$ (the 'dirty limit') the second term dominates and $B_{C2}(0) \propto \gamma T_C$. For intermediate values of $\lambda_{tr}$, $B_{C2}(0)$ is approximately proportional to $(\gamma T_C)^v$, where the exponent $v$ depends only on $\lambda_{tr}$ and has a value between ∼1 and ∼2. The variation of $\gamma$ with $T_C$ (see figure 10) is such that an approximate power-law relationship between $B_{C2}(0)$ and $T_C$ is also obtained (equation (8)), with an exponent ($w$) that depends on $\lambda_{tr}$ and on the relative contribution of electronic and phononic changes. Figure 11 shows a normalized log–log plot of the calculated values of $B_{C2}(0, \varepsilon_I)$ as a function of $T_C(\varepsilon_I)$ for $Nb_3Sn$. It can be seen that the relationship is indeed quite accurately described by a power law with, for $\lambda_{tr}(\varepsilon_I = 0) = 3$, the exponent $w = 2.4$ for the case where only $\omega_{ln}$ varies with uniaxial strain, and $w = 3.0$ for the case where only $N(0)$ varies with strain. These values are for fits over the range $0.77 \leqslant T_C(\varepsilon_I)/T_C(0) \leqslant 1$, which is relevant for comparison with our experimental data in figure 9 although $w$ can vary depending on the exact temperature range chosen

by about $\pm 0.1$. The deviations from the power law are such that $w$ is larger (by $\leqslant 0.6$) closer to $T_C(\varepsilon_I)/T_C(0) = 1$. We have investigated alternative functional forms that describe the theoretical data in figure 11 rather better, but have not used them in this paper because the power law is reasonably accurate for both clean and dirty superconductors and the improvement in $J_C$ parametrization was not sufficiently large. Given the large uncertainties in $\lambda_{tr}$, we have also shown in figure 11 the results and values of $w$ for $\lambda_{tr}(\varepsilon_I = 0) = 5.5$ and 1 (1 is considered as the lower bound for $Nb_3Sn$ with $B_{C2}(0, \varepsilon_I = 0) \geqslant 27$ T), as well as for the extreme dirty limit ($\lambda_{tr} = \infty$). It can be seen that $w$ increases as $\lambda_{tr}(\varepsilon_I = 0)$ decreases or the relative contribution of variations in $N(0)$ increases. If the Kresin equation for $T_C$ is used instead of the Allen and Dynes equation then the values of $w$ obtained are lower by typically 0.1. Similar results are obtained using data from measurements on $Nb_3Al$ thin films [78] that imply $\lambda_{tr} \approx 7$, corresponding to $w \approx 2.5$ (variations only in $\omega_{ln}$) and $w \approx 2.9$ (variations only in $N(0)$) for the range $T_C(\varepsilon_I)/T_C(0) \geqslant 0.92$ ($\varepsilon_I = -1.4\%$ for the jelly-roll $Nb_3Al$ wire).

### 4.3. Comparison of theoretical and experimental results

Comparing the theoretical values for $w$ (figure 11) with the experimental data (figure 9), it can be seen that the agreement is considerably better if the strain dependence of the average phonon frequencies is the dominant factor. Assuming $\lambda_{tr}(\varepsilon_I = 0) = 3$, microscopic theory gives $w = 2.4$ if $N(0)$ is constant (and higher values if $N(0)$ varies) which can be compared to the typical experimental values for high-$B^*_{C2}(0)$ wires between $\sim 2$ and $\sim 2.5$. Our results are therefore in agreement with the implications of Testardi's work [43–45], who related the strain dependence of $T_C$ to the large phonon anharmonicity effects in $A15$ superconductors [80, 81]. Recent work also shows that the strain dependence of the critical temperature in $Nb_3Sn$ can be explained using a 3D model which assumes that changes only occur in the phonon spectrum [35]. Alternatively, various properties of $A15$ compounds have been related to peaks in the electronic density of states near the Fermi energy [82, 83]. However, it has been noted that tertiary additions would broaden these peaks and therefore cause a reduction in the strain-sensitivity of $T_C$ if the variations in $N(0)$ were indeed the dominant factor, whereas the opposite effect is observed experimentally (see figure 8(a)) [42]. Band-structure calculations [84–86] also show that there is only a relatively small decrease in $N(0)$ ($<3\%$) for the transition from the cubic to the tetragonal phases of $Nb_3Sn$. Here, the distortion of the unit cell in the tetragonal phase [45] can be considered as equivalent to a macroscopic strain of $\varepsilon_I \approx -0.44\%$ (calculated by equating the deviatoric strain components [17]): the lower values of $T_C$ ($\sim 1$ K in otherwise equivalent materials) [87] and $B_{C2}(0)$ ($\sim 3$ T) [77] observed for the tetragonal phase are indeed broadly consistent with our strain results (see figure 8).

Some other results in the literature can be used to assess the validity of the assumptions made in the analysis and the conclusions about the microscopic mechanism. Due to a lack of information about uniaxial strain effects, it is necessary to discuss measurements of microscopic properties as a function of various other adjustable parameters. In measurements on $Nb_3Sn$ under hydrostatic pressure [19], changes in both $N(0)$ and $\omega_{ln}$ were observed, and the parameter $\langle I^2 \rangle$ increased slightly as $N(0)$ decreased (in contrast to our assumption of $\langle I^2 \rangle$ = constant). The large differences between the effect of non-hydrostatic (uniaxial) strains and hydrostatic strains on the superconducting properties ($T_C$) [14] may indicate that there is a different mechanism operating in each case (indeed, the dependences are of opposite sign in $V_3Si$ [42, 88]). Nevertheless, such a correlation between $N(0)$ and $\langle I^2 \rangle$ [89] would tend to increase the calculated value of $w$ and therefore, from the comparison with the experimental data, further strengthen the case for phononic changes being the dominant factor. We also note that experimental [90] and computational [91] data show that $\langle I^2 \rangle$ is approximately constant for series of different niobium-based superconductors. Tunnelling measurements [73] on Nb–Sn samples with varying stoichiometry show that $\mu^*$ is approximately constant for variations in $T_C$ of $\sim 7$ K, consistent with our assumption for the case of uniaxial strain. In these measurements, the largest changes in $\alpha^2 F(\omega)$ occurred at lower frequencies and therefore $\omega_{ln}$ varied more than $\omega_2$ (by $\sim 50\%$ for variations in $T_C$ of $\sim 3$ K): this effect would also tend to increase the calculated value of $w$ (and further emphasize the role of phononic changes).

Comparison between our experimental data and theory provides strong evidence that in high-$B^*_{C2}$ $Nb_3Sn$ uniaxial strain predominantly changes the average phonon frequencies rather than the electronic density of states at the Fermi energy. The theory—in which $w$ decreases with increasing impurity scattering rate—also provides a straightforward explanation for low values of $w$ ($\leqslant 2.5$) for ternary $Nb_3Sn$ compared to the binary materials ($\sim 3.6$) [6, 11]. Estimating $\lambda_{tr} \approx 1$ for the binary $Nb_3Sn$ wires [79], and considering values of $T_C(\varepsilon_I)/T_C(0) \geqslant 0.94$, gives $w \approx 3.3$ for the case where phononic changes dominate and $w \approx 3.9$ for the case where the electronic changes dominate.

## 5. A scaling law for $J_C(B, T, \varepsilon)$

Using the phenomenological framework (section 3) and the results of microscopic theory (section 4), we propose a scaling law for $J_C(B, T, \varepsilon)$ including equations (5) and (7) together with equation (8) (the power-law relationship between $B^*_{C2}(0, \varepsilon_I)$ and $T^*_C(\varepsilon_I)$), which is taken to be valid for different electron–phonon coupling strengths and impurity scattering rates. We propose parametrizing $B^*_{C2}(0, \varepsilon_I)$ by the following expression:

$$\frac{B^*_{C2}(0, \varepsilon_I)}{B^*_{C2}(0, 0)} = 1 + c_2\varepsilon_I^2 + c_3\varepsilon_I^3 + c_4\varepsilon_I^4, \qquad (14)$$

and using equation (8) to calculate $T^*_C(\varepsilon_I)$. Figure 8 shows that decreases in the strain sensitivity of $T^*_C(\varepsilon_I)$ are correlated with increases in the exponent $w$, which is consistent with the data for binary and ternary $Nb_3Sn$ and is sufficient to produce an approximately universal relationship for $B^*_{C2}(0, \varepsilon_I)$ for the ternary data presented in this paper. Hence the parametrization of $B^*_{C2}(0, \varepsilon_I)$ is expected to be less sensitive to the compositional variations that occur in technological superconductors.

**Table 2.** RMS errors for fits to the comprehensive $J_C(B, T, \varepsilon)$ data using various scaling laws.

| Scaling law | RMS error (mean $I_C$) (A) | | |
|---|---|---|---|
| | Internal-tin wire | Bronze-route wire | MJR wire |
| | (42.5) | (61.4) | (35.7) |
| ISL [5] | 1.40 | 2.05 | 1.35 |
| $u$ free | 1.40 | 2.50 | 1.68 |
| $u = 0$ | 1.40 | 2.50 | 1.81 |
| $u = 1.25$ | 1.55 | 3.20 | 2.33 |
| $A(0)$, $T_C^*(0)$, $B_{C2}^*(0, 0)$, $\varepsilon_M$ free | 2.10 | 6.60 | 5.71 |

We also include in the scaling law the following power-law relationship between $A(\varepsilon_I)$ and $T_C(\varepsilon_I)$:

$$\frac{A(\varepsilon_I)}{A(0)} = \left(\frac{T_C^*(\varepsilon_I)}{T_C^*(0)}\right)^u, \tag{15}$$

as proposed by Summers [28]. Using equations (4), (6) and (7), the prefactor $A(\varepsilon_I)$ can be written as

$$A(\varepsilon_I) = 0.97\mu_0^{1/2} A'(\varepsilon_I)\gamma(\varepsilon_I)/\eta(\varepsilon_I). \tag{16}$$

The results from microscopic theory presented in section 4.2 allow the term $\gamma(\varepsilon_I)/\eta(\varepsilon_I)$ in equation (16) to be related to $T_C^*(\varepsilon_I)$. Assuming that $A'(\varepsilon_I) =$ constant, an approximate power-law relationship between $A(\varepsilon_I)$ and $T_C^*(\varepsilon_I)$ is then obtained with an exponent $u$ that is independent of scattering rate and equal to 1.25 (variations only in $\omega_{ln}$) or 1.65 (variations only in $N(0)$). As shown in table 2, however, the fits to the complete datasets using the scaling law with $u = 1.25$ have RMS errors that are ∼30% higher than the fits with $u$ as a free parameter. The optimum values for $u$ are approximately zero for the internal-tin and bronze-route wires and approximately −1 for the MJR wire, although the latter value has a large associated uncertainty, as shown by the small increase in the error that is observed when $u$ is fixed at zero (see table 2). Hence the large uncertainties in $u$ (and our assumption about the value of $m$) prevent any definite physical interpretation of $A'(\varepsilon_I)$ at this stage [13, 26]. The optimum values of $u$ in the scaling law can be compared with the Summers scaling law, in which the variation of the prefactor was fixed so that $F_{PM}(0, \varepsilon_I) \propto [B_{C2}^*(0, \varepsilon_I)]^{n'}$ with $n' = 1$, in approximate agreement with Ekin's strain scaling law ($F_{PM}(0, \varepsilon_I)$ is the maximum volume pinning force at $T = 0$) [6, 28]. In the scaling law, $n' = w^{-1}[u + 2 + w(n - 2)]$ and has values of ∼1.1 (internal tin) and ∼1.2 (bronze route).

Using equations (5), (7), (8), (14) and (15) to fit the complete $J_C(B, T, \varepsilon)$ datasets for the bronze-route, internal-tin and MJR [5] $Nb_3Sn$ wires gives RMS errors of ∼1.5–2.5 A, as shown in table 2. The scaling law involves 13 free parameters (compared to 17 for the ISL), the optimum values of which are shown in table 3.

Universal values for the scaling-law parameters are required to make predictions of $J_C(B, T, \varepsilon)$ based on partial datasets (e.g. from measurements at single values of temperature and/or strain). Table 4 shows a set of universal values proposed for ternary, high-upper-critical-field $Nb_3Sn$. These include the Kramer values of $p = 1/2$ and $q = 2$ [26, 27], a value of $\nu = 3/2$ that approximately describes (to within ∼2%) the Maki–de Gennes relation

**Table 3.** Scaling-law parameters for (a) the MJR (OST) wire, (b) the bronze-route (Vac) wire and (c) the internal-tin (EM-LMI) $Nb_3Sn$ wire. Note that for the values given in the table intrinsic strain is in units of % and the calculated $J_C$ is the engineering critical current density in units of A m$^{-2}$.

| (a) MJR wire | | | | | | |
|---|---|---|---|---|---|---|
| $p$ | $q$ | $n$ | $\nu$ | $w$ | $u$ | $\varepsilon_M$ (%) |
| 0.4763 | 2.150 | 3.069 | 1.240 | 2.545 | −0.912 | 0.2421 |
| $A(0)$ (A m$^{-2}$ T$^{3-n}$ K$^{-2}$) | $T_C^*(0)$ (K) | | $B_{C2}^*(0, 0)$ (T) | $c_2$ | $c_3$ | $c_4$ |
| $6.417 \times 10^6$ | 18.00 | | 29.17 | −0.6457 | −0.4514 | −0.1009 |
| (b) Bronze-route wire | | | | | | |
| $p$ | $q$ | $n$ | $\nu$ | $w$ | $u$ | $\varepsilon_M$ (%) |
| 0.4625 | 1.452 | 2.457 | 1.225 | 2.216 | 0.051 | 0.3404 |
| $A(0)$ (A m$^{-2}$ T$^{3-n}$ K$^{-2}$) | $T_C^*(0)$ (K) | | $B_{C2}^*(0, 0)$ (T) | $c_2$ | $c_3$ | $c_4$ |
| $9.460 \times 10^6$ | 17.58 | | 29.59 | −0.6602 | −0.4656 | −0.1075 |
| (c) Internal-tin wire | | | | | | |
| $p$ | $q$ | $n$ | $\nu$ | $w$ | $u$ | $\varepsilon_M$ (%) |
| 0.4741 | 1.953 | 2.338 | 1.446 | 1.936 | −0.056 | 0.2786 |
| $A(0)$ (A m$^{-2}$ T$^{3-n}$ K$^{-2}$) | $T_C^*(0)$ (K) | | $B_{C2}^*(0, 0)$ (T) | $c_2$ | $c_3$ | $c_4$ |
| $2.446 \times 10^7$ | 16.89 | | 28.54 | −0.7697 | −0.4913 | −0.0538 |

**Table 4.** Approximate universal values for the scaling law parameters in order to fit partial $J_C(B, T, \varepsilon)$ datasets for ternary $Nb_3Sn$ wires, including the coefficients of a fifth-order polynomial for normalized $B^*_{C2}(0)$ ($c_0 = 1, c_1 = 0$). The values on the top row can be used for various types of partial dataset (e.g. variable-strain data at 4.2 K combined with variable-temperature data at zero applied strain). If only variable-strain data are available, a value of $T^*_C(0) \approx 17.5$ K is also required. All of the values can be used if only variable-temperature data are available (in which case an estimate of $\varepsilon_M$ is also required [93, 94]).

| $p$ | $q$ | $n$ | $\nu$ | $w$ |
|---|---|---|---|---|
| 0.5 | 2 | 2.5 | 1.5 | 2.2 |
| $u$ | $c_2$ | $c_3$ | $c_4$ | $c_5$ |
| 0 | −0.752 | −0.419 | 0.0611 | 0.0619 |

for $B_{C2}(T)$ [39, 64, 65], and a half-integral value of $n = 5/2$ observed for a number of $Nb_3Sn$ wires [3, 5]. The universal relation for the normalized values of $B^*_{C2}(0, \varepsilon_I)$ shown in figure 8(a) can be described by a fifth-order polynomial with values for the coefficients as shown in table 4. Based on our comprehensive data for the internal-tin, bronze-route and MJR wires, and consistent with microscopic theory, we propose the universal value of $w = 2.2$. Variations in $w$ of approximately ±20% are observed (and are expected due to variations in the dirtiness of the $Nb_3Sn$). Given the accuracy of the fits shown in table 2, we also propose a value of $u = 0$ (i.e. $A(\varepsilon_I) = \text{const}$). It can be seen by comparing tables 3 and 4 that there are some differences between the optimum and universal values for the scaling-law exponents, particularly for the bronze-route wire where the assumption that $p = 1/2$ and $q = 2$ leads to unphysically high values for the effective upper critical field (∼35 T). The fits to the complete $J_C(B, T, \varepsilon)$ datasets using the set of universal parameters (i.e. with $A(0)$, $B^*_{C2}(0, 0)$, $T^*_C(0)$ and $\varepsilon_M$ as the free parameters) have RMS errors that are ∼5–15% of the mean critical current (see table 2). We have completed a comprehensive analysis of the parametrization of partial datasets and have noted in table 4 the optimal use of the universal values that enable similar levels of accuracy to be achieved when extrapolating from partial datasets.

## 6. Conclusions

Comprehensive $J_C(B, T, \varepsilon)$ data are presented for the internal-tin (EM-LMI) and bronze-route (Vac) $Nb_3Sn$ superconducting wires used in the two ITER model coils. Various consistency tests demonstrate good interlaboratory agreement and that $J_C$ is a single-valued function of $B$, $T$ and $\varepsilon$. For high-upper-critical-field (28–30 T) $Nb_3Sn$ wires, we report an approximately universal relationship between normalized $B^*_{C2}(0)$ and intrinsic strain, and a power-law relationship between $B^*_{C2}(0, \varepsilon_I)$ and $T^*_C(\varepsilon_I)$ with a typical value of ∼2.2 for the exponent. Both results differ from those obtained previously for binary, low-upper-critical-field (∼24 T) $Nb_3Sn$ wires in which $B^*_{C2}(0)$ and $T^*_C$ are less strain dependent and the power-law exponent is larger ($\geqslant 3$). The standard Summers scaling law therefore predicts a weaker strain dependence for $J_C$ and does not accurately fit the $J_C(B, T, \varepsilon)$ data for the internal-tin or bronze-route wires. Analysis of the relationship between $B^*_{C2}(0, \varepsilon_I)$ and $T^*_C(\varepsilon_I)$ using microscopic theory shows that the calculated value for the power-law exponent decreases with increasing impurity scattering rate in agreement with the experimental data, and that the uniaxial strain effects are predominantly due to changes in the average phonon frequencies rather than the electronic density of states at the Fermi energy. We propose a scaling law to describe $J_C(B, T, \varepsilon)$ in technological $Nb_3Sn$ wires with high values of upper critical field, motivated by microscopic theory and phenomenological scaling. The scaling law incorporates a polynomial function for normalized $B^*_{C2}(0, \varepsilon_I)$ and modified power-law relations between the strain-dependent variables. It allows accurate (∼4%) parametrizations to be made of complete $J_C(B, T, \varepsilon)$ datasets and, with appropriate universal values for some of the parameters, reasonably accurate predictions to be made from partial datasets.

## Acknowledgments

We would like to thank Eric Mossang for assistance with the very high field measurements in Grenoble, Matthew Pritchard and Paul Foley for assistance with various experimental tasks, and Jean-Luc Duchateau, Neil Mitchell, Arend Nijhuis, Kozo Osamura, Alfredo Portone, Ettore Salpietro, Alexander Vostner and Roberto Zanino for valuable discussions. This work was supported by the EFDA/ITER program, EPSRC, Oxford Instruments PLC and the Japanese NEDO Grant project (Applied Superconductivity, 2004EA004).

## References

[1] Miyazaki T, Hase T and Miyatake T 2003 *Handbook of Superconducting Materials* vol 2, ed D Cardwell and D Ginley (Bristol: Institute of Physics Publishing) pp 639–72
[2] ten Haken B, Godeke A and ten Kate H H J 1999 *J. Appl. Phys.* **85** 3247–53
[3] Hampshire D P, Jones H and Mitchell E W J 1984 *IEEE Trans. Magn.* **21** 289–92
[4] Martínez A and Duchateau J L 1997 *Cryogenics* **37** 865–75
[5] Keys S A and Hampshire D P 2003 *Supercond. Sci. Technol.* **16** 1097–108
[6] Ekin J W 1980 *Cryogenics* **20** 611–24
[7] Easton D S and Schwall R E 1976 *Appl. Phys. Lett.* **29** 319–21
[8] Buehler E and Levinstein H J 1965 *J. Appl. Phys.* **36** 3856
[9] Ekin J W 1976 *Appl. Phys. Lett.* **29** 216–9
[10] McDougall I L 1975 *IEEE Trans. Magn.* **11** 1467–9
[11] Luhman T, Suenaga M and Klamut C J 1978 *Adv. Cryog. Eng.* **24** 325–30
[12] Rupp G 1979 *IEEE Trans. Magn.* **15** 189–92
[13] Kroeger D M *et al* 1980 *J. Appl. Phys.* **51** 2184–92
[14] Welch D O 1980 *Adv. Cryog. Eng.* **26** 48–65
[15] Ekin J W 1987 *J. Appl. Phys.* **62** 4829–34
[16] Katagiri K *et al* 1995 *IEEE Trans. Appl. Supercond.* **5** 1900–4
[17] Godeke A, ten Haken B and ten Kate H H J 2002 *Physica* C **372–376** 1295–8
[18] ten Haken B, Godeke A and ten Kate H H J 1995 *Proc. EUCAS 1995, the 2nd European Conf. on Applied Superconductivity* ed D Dew-Hughes (Bristol: Institute of Physics Publishing) pp 85–8
[19] Lim K C, Thompson J D and Webb G W 1983 *Phys. Rev.* B **27** 2781–7
[20] Aymar R 2001 *Fusion Eng. Des.* **55** 107–18
[21] Zanino R and Savoldi-Richard L 2003 *Cryogenics* **43** 79–90
[22] Mitchell N 2003 *Fusion Eng. Des.* **66–68** 971–93
[23] Zanino R and Savoldi-Richard L 2003 *Cryogenics* **43** 91–100

[24] Zanino R, Mitchell N and Savoldi-Richard L 2003 *Cryogenics* **43** 179–97
[25] Fietz W A and Webb W W 1969 *Phys. Rev.* **178** 657–67
[26] Dew-Hughes D 1974 *Phil. Mag.* **30** 293–305
[27] Kramer E J 1973 *J. Appl. Phys.* **44** 1360–70
[28] Summers L T *et al* 1991 *IEEE Trans. Magn.* **27** 2041–4
[29] Godeke A and Knoopers H G 1998 *University of Twente Report No.* UT-NET 98-5
[30] Cheggour N and Hampshire D P 1999 *J. Appl. Phys.* **86** 552–5
[31] Keys S A, Koizumi N and Hampshire D P 2002 *Supercond. Sci. Technol.* **15** 991–1010
[32] Allen P B and Dynes R C 1975 *Phys. Rev.* B **12** 905–22
[33] Bardeen J, Cooper L N and Schrieffer J R 1957 *Phys. Rev.* **108** 1175–204
[34] McMillan W L 1968 *Phys. Rev.* **167** 331–44
[35] Markiewicz W D 2004 *Cryogenics* **44** 895–908
[36] Kresin V Z, Gutfreund H and Little W A 1984 *Solid State Commun.* **51** 339–42
[37] Kresin V Z 1987 *Phys. Lett.* A **122** 434–8
[38] Kresin V Z, Morawitz H and Wolf S A 1993 *Mechanisms of Conventional and High $T_c$ Superconductivity* (New York: Oxford University Press)
[39] Helfand E and Werthamer N R 1966 *Phys. Rev.* **147** 288–94
[40] Carbotte J P 1990 *Rev. Mod. Phys.* **62** 1027–157
[41] Orlando T P *et al* 1979 *Phys. Rev.* B **19** 4545–61
[42] Ekin J W 1984 *Adv. Cryog. Eng.* **30** 823–36
[43] Testardi L R 1975 *Rev. Mod. Phys.* **47** 637–48
[44] Testardi L R 1972 *Phys. Rev.* B **5** 4342–9
[45] Testardi L R 1973 *Physical Acoustics* vol 10, ed W P Mason and R N Thurston (New York: Academic) p 193
[46] Taylor D M J and Hampshire D P 2003 *Physica* C **401** 40–6
[47] Walters C R, Davidson I M and Tuck G E 1986 *Cryogenics* **26** 406–12
[48] Taylor D M J and Hampshire D P 2005 *Supercond. Sci. Technol.* **18** 356–68
[49] Cheggour N and Hampshire D P 2000 *Rev. Sci. Instrum.* **71** 4521–30
[50] Brandt B L, Liu D W and Rubin L G 1999 *Rev. Sci. Instrum.* **70** 104–10
[51] Keys S A and Hampshire D P 2003 *Handbook of Superconducting Materials* vol 2, ed D Cardwell and D Ginley (Bristol: Institute of Physics Publishing) pp 1297–322
[52] Rupp G 1980 *Filamentary A15 Superconductors* ed M Suenaga and A F Clark (New York: Plenum) p 155
[53] Hampshire D P *et al* 2001 *University of Durham Report No.* DurSC0601
[54] Uglietti D *et al* 2003 *Supercond. Sci. Technol.* **16** 1000–4
[55] Specking W, Duchateau J L and Decool P 1998 *Proc. 15th Int. Conf. on Magnet Technology* ed L Liangzhen, S Guoliao and Y Luguang (Beijing: Science Press) pp 1210–3
[56] Zanino R *et al* 2004 *IEEE Trans. Appl. Supercond.* **14** 1519–22
[57] Taylor D M J, Keys S A and Hampshire D P 2002 *Physica* C **372** 1291–4
[58] Anderson P W and Kim Y B 1964 *Rev. Mod. Phys.* **36** 39–43
[59] Goodrich L F, Medina L T and Stauffer T C 1998 *Adv. Cryog. Eng.* **44** 873–80
[60] Küpfer H and Gey W 1977 *Phil. Mag.* **36** 859–84
[61] Sneary A B *et al* 1999 *IEEE Trans. Appl. Supercond.* **9** 2585–8
[62] Goodrich L F and Stauffer T C 2001 *IEEE Trans. Appl. Supercond.* **11** 3234–7
[63] ITER Organisation 2002 *Design Requirements and Guidelines Level 1* (Annex)
[64] De Gennes P G 1964 *Phys. Kondens. Mater.* **3** 79
[65] Maki K 1964 *Physics* **1** 21–30
[66] Lee P J and Larbalestier D C 2001 *IEEE Trans. Appl. Supercond.* **11** 3671–4
[67] Godeke A *et al* 2003 *Supercond. Sci. Technol.* **16** 1019–25
[68] Cooley L D *et al* 2004 *J. Appl. Phys.* **96** 2122–30
[69] ten Haken B, Godeke A and ten Kate H H J 1995 *IEEE Trans. Appl. Supercond.* **5** 1909–12
[70] Wang S T *et al* 1994 *IEEE Trans. Magn.* **30** 2344–7
[71] Wolf E L *et al* 1980 *Phys. Rev.* B **22** 1214–7
[72] Kwo J and Geballe T H 1981 *Phys. Rev.* B **23** 3230–9
[73] Rudman D A and Beasley M R 1984 *Phys. Rev.* B **30** 2590–4
[74] Markiewicz W D 2004 *Cryogenics* **44** 767–82
[75] Werthamer N R, Helfand E and Hohenberg P C 1966 *Phys. Rev.* **147** 295–302
[76] Schossmann M and Schachinger E 1986 *Phys. Rev.* B **33** 6123–31
[77] Foner S and McNiff E J 1981 *Solid State Commun.* **39** 959–64
[78] Kwo J, Orlando T P and Beasley M R 1981 *Phys. Rev.* B **24** 2506–14
[79] Suenaga M *et al* 1986 *J. Appl. Phys.* **59** 840–53
[80] Patel J R and Batterman B W 1966 *Phys. Rev.* **148** 662–4
[81] Poirier M *et al* 1985 *Appl. Phys. Lett.* **47** 92–4
[82] Weger M and Goldberg I B 1973 *Solid State Physics* vol 28, ed H Ehrenreich, F Seitz and D Turnbull (New York: Academic) pp 1–177
[83] Klein B M *et al* 1979 *Phys. Rev.* B **18** 6411–38
[84] Weber W and Mattheiss L F 1982 *Phys. Rev.* B **25** 2270–84
[85] Sadigh B and Ozolins V 1998 *Phys. Rev.* B **57** 2793–800
[86] Mattheiss L F and Weber W 1982 *Phys. Rev.* B **25** 2248–69
[87] Vieland L J and Wicklund A W 1971 *Phys. Lett.* A **34** 43–4
[88] Chu C W and Diatschenko V 1978 *Phys. Rev. Lett.* **41** 572–5
[89] Hopfield J J 1969 *Phys. Rev.* **186** 443–51
[90] Junod A, Jarlborg T and Muller J 1983 *Phys. Rev.* B **27** 1568–85
[91] Klein B M, Boyer L L and Papaconstantopoulos D A 1979 *Phys. Rev. Lett.* **42** 530–3
[92] Godeke A and Krooshoop H J G 2000 *University of Twente Report No.* UT-NET/EFDA 2000-5
[93] Ochiai S, Osamura K and Watanabe K 1993 *J. Appl. Phys.* **74** 440–5
[94] Easton D S *et al* 1980 *J. Appl. Phys.* **51** 2748–57